RSC Advances

Check for updates

Synergistic effects boosting hydrogen evolution performance of transition metal oxides at ultralow Ru loading levels†

Miao Yang, [iD] *[a] Hong Yang,[a] Feng Wang,[a] Yulan Niu*[a] and Pan Li*[b]

In this study, ultralow ruthenium nanoparticles on the nickel molybdate nanorods grown on nickel foam (Ru–NiMoO$_4$–NF) were synthesized. The Ru–NiMoO$_4$–NF exhibited outstanding hydrogen evolution reaction performances in alkaline with overpotential of 52 mV at the current density of 10 mA cm^{-2}. And, it maintains excellent stability for 20 h at the current density of 20 mA cm^{-2}. The mass activity of Ru–NiMoO$_4$–NF is 0.21 A mg$_{Ru}^{-1}$, which is higher than that of Pt/C. Lots of exposed heterojunction interfaces and synergistic effects between Ru nanoparticles and NiMoO$_4$ nanorods were regarded as the reasons for excellent performance. This work provides an innovative route for developing low-cost catalysts based on the transition metal oxides and trace precious metal with unique heterostructures for hydrogen production through water splitting.

Introduction

Hydrogen (H$_2$) is one of the most promising clean energy due to its high energy density and zero carbon dioxide (CO$_2$) emissions after combustion.[1,2] Nowadays, hydrogen production *via* electrochemical water splitting can effectively minimize environmental pollution and energy consumption, which is widely recognized as a promising carbon-neutral technology.[3–6] The water electrolysis consists of hydrogen evolution reactions (HER) and oxygen evolution reactions (OER), which can operate in either alkaline or acid conditions.[7–9] While, industry-compatible large-scale hydrogen production is based on alkaline water electrolysis.[10–13] However, the alkaline HER is more sluggish than that in acidic media, which requires considerable energy to break the HO–H bond to produce protons.[14–17] Therefore, developing efficient electrocatalysts to enhance water dissociation and hydrogen desorption is highly desirable.[18,19]

Noble metal platinum-based catalysts are regarded as the state-of-the-art electrocatalysts for HER, ascribing to its optimal hydrogen adsorption free energy.[20,21] But, the low reserves, high cost, and inferior activity for water dissociation limited their application in alkaline conditions.[22] As cheaper alternatives to platinum, ruthenium-based electrocatalysts with similar metal–hydrogen binding energy and relatively higher reserves have

attracted considerable research interest.[14,23,24] The ultrafine Ru nanoclusters anchored on the N-doped nanoporous carbon afford unprecedented performance for HER.[25] To study the sized-dependent activity of Ru nanocrystals, a series of Ru nanoparticles and clusters were synthesized by He's group.[14] They discovered that the subnanometric Ru clusters with unique physicochemical features displayed excellent HER electrocatalytic performance. However, the pure ruthenium catalyst delivered inferior hydrogen evolution in alkaline environment because of the poor water decomposition ability and strong hydrogen adsorption. Therefore, exploring Ru nanomaterials with other strong water dissociation ability components are desired to achieve the perfect hydrogen evolution activity. The latest research shows that non-noble transition metal oxides (TMOs) are abundant reserves and effective for the HO–H bond rupture in water.[26–30] Hence, combining with the TMOs and Ru-based materials should be the active electrocatalysts for HER in alkaline. For instance, the Ru–MoO$_2$ nanocomposites reported by Q. Chen *et al.* exhibited Pt-like electrocatalytic behavior with very low overpotential of 29 mV at 10 mA cm^{-2} in 1 M KOH.[31] Shi Hu and coworkers synthesized densely packed NiO@Ru nanosheets, which exhibited intimate interface contact of NiO and Ru, super-hydrophilic surface structure, and low charge transfer resistance for excellent HER performance.[32] Besides, it was also shown that integration of NiFe LDH with sub-nanoscale Ru species can dramatically optimize the adsorption energy of H* and improve the HER kinetics.[33] Considering these above views, the appropriate design of electrocatalysts with synergistic effects would achieve superb HER performance in alkaline.

A particular challenge is how to construct TMOs and Ru-based materials in intimate contact and expose large areas.

[a] Collaborative Innovation Center of CO$_2$ Conversion and Utilization, Department of Chemistry and Chemical Engineering, Taiyuan Institute of Technology, Taiyuan Shanxi, 030008, P. R. China. E-mail: m_miaoyang@163.com; niuyl@tit.edu.cn

[b] Department of Environment and Safety Engineering, Taiyuan Institute of Technology, Taiyuan Shanxi, 030008, P. R. China. E-mail: lipan201104@163.com

† Electronic supplementary information (ESI) available. See DOI: https://doi.org/10.1039/d3ra01501g

Generally speaking, α-NiMoO$_4$ has high stability, poor conductivity, and low catalytic activity, while β-NiMoO$_4$ is metastable but has high catalytic activity. How to improve the activity of α-NiMoO$_4$ catalyst is a great challenge at present.[28,30,34] In this work, ultralow Ru was introduced into α-NiMoO$_4$–NF nanorods, and the catalytic activity was improved through the synergistic effect of two components and the improvement of the conductivity. Meantime, the nanorods array structure could promote the directional transfer of electron along the array direction. Ru nanoparticles were grown on the α-NiMoO$_4$–NF nanorods by ion-exchange strategy (shorthand for Ru–NiMoO$_4$–NF). The unique heterostructures between Ru nanoparticles and α-NiMoO$_4$ nanorods resulted in remarkable HER catalytic activity in alkaline solutions. Notably, the overpotential of Ru–NiMoO$_4$–NF is only 52 mV@10 mA cm^{-2} for alkaline HER, with Tafel slope of 45 mV dec^{-1} and mass activity of 0.21 A mg$_{Ru}^{-1}$. Thus, this work establishes an innovative strategy to boost HER activity with ultralow Ru loading in TMOs.

Results and discussion

The Ru–NiMoO$_4$–NF catalyst was synthesized *via* two-step solvothermal approach (details in the Experimental section in ESI†). Briefly, nickel molybdate hydrate nanorods precursor

supported on nickel foam (abbreviation for NiMoO$_4$–NF) was firstly grown on the nickel foam *via* hydrothermal method.[34] The synthesized solid nickel molybdate hydrate nanorod arrays were immersed in RuCl$_3$ ethanol solution at 100 °C for 15 h to obtain Ru–NiMoO$_4$–NF nanorods through an ion-exchange strategy. The scanning electron microscope (SEM) and transmission electron microscope (TEM) were used to deeply investigate the morphologies and microstructures of these catalysts. As illustrated in ESI Fig. S1,† the pure nickel form with a three-dimensional (3D) skeleton structure could expose more surface area and increase the contact interface between the electrolyte and electrode. After the hydrothermal reaction in Ni(NO$_3$)$_2$ and NaMoO$_2$ aqueous solution, the NiMoO$_4$ nanorods with smooth surfaces were vertically grown on the nickel foam as shown in Fig. 1a, b, and S2.† After the introduction of Ru, the nanorod arrays kept unchanged, but the surface became rough, with uniform decoration of Ru nanoparticles (Fig. 1c and d). As displayed in Fig. 2a–h, high-resolution TEM images revealed that the nanoparticles anchored on the nanorod were the Ru nanoparticles. The magnified images of Ru–NiMoO$_4$ exhibit clear lattice fringes with an interplanar spacing of 0.873 nm in nanorod, which was assigned to the (001) plane of NiMoO$_4$. As shown in Fig. 2b and c, the intimate contact between NiMoO$_4$ nanorod and Ru nanoparticles could efficiently accelerate electron transfer by the interface mutual interaction during the electrocatalytic process. In addition, elemental mappings based on the HADDF-STEM images (Fig. 2d–h) demonstrated the elements of Mo, O, and Ni distribute uniformly, while the element of Ru was mainly located in the part of nanoparticles. Concomitantly, as shown in Fig. S3,† the energy-dispersive spectrometer (EDS) illustrated the element content of Ru–NiMoO$_4$. The weight ratio of O, Ni, Mo, and Ru was 18.83%, 34.75%, 44.06%, and 2.36%, respectively. Furthermore, the element content of Ru–NiMoO$_4$–NF was collected by inductively coupled plasma-optical emission spectrometer (ICP-OES). The results indicated that the mass content of Ru is about 2.1 wt%, confirming the successful doping of Ru. N$_2$ adsorption–desorption isotherms of Ru–NiMoO$_4$–NF and NiMoO$_4$–NF (Fig S4†) were tested. The BET surface area of Ru–NiMoO$_4$–NF and
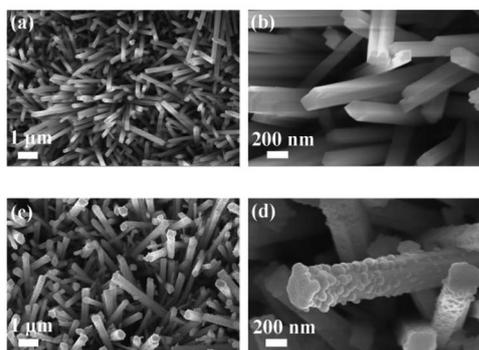

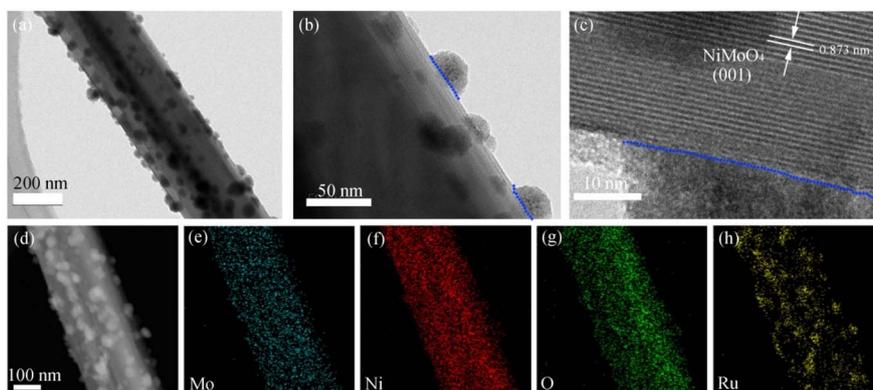**Fig. 1** SEM images of (a, b) NiMoO$_4$–NF and (c, d) of Ru–NiMoO$_4$–NF.

Fig. 2 (a and b) TEM; (c) HRTEM; (d–h) HAADF and elemental mapping images of Ru–NiMoO$_4$–NF.
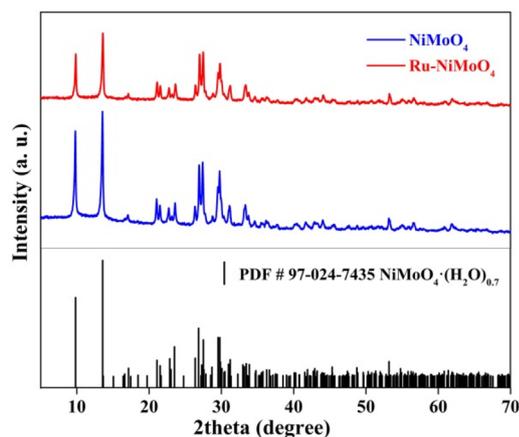
Fig. 3 XRD patterns of $NiMoO_4$ and $Ru–NiMoO_4$.

$NiMoO_4$–NF are 5.03 m^2 g^{-1} and 3.43 m^2 g^{-1}, indicating the increase of specific surface area after the introduction of Ru.

X-ray powder diffraction (XRD) and X-ray photoelectron spectra (XPS) of the prepared samples were obtained to analyze the crystal structure and surface electronic structures. Fig. 3 illustrated the XRD patterns of $NiMoO_4$ and $Ru–NiMoO_4$ catalysts scraped from the Nickel Foam surface. The XRD patterns indicated that the catalysts of α-$NiMoO_4$ (PDF No. 97-024-7435) were successfully synthesized on Nickel Foam. However, with the introduction of Ru, XRD diffraction peaks of the catalysts did not change, indicating that no crystalized Ru metals and oxides were formed. Ru may exist in an amorphous state. The survey XPS spectrum (Fig. 4a) of $Ru–NiMoO_4$–NF shows the

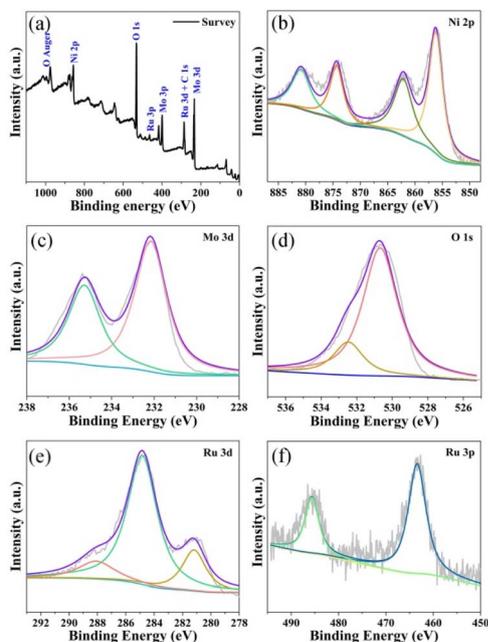coexistence of Ru, Ni, Mo, and O elements. As depicted in Fig. 4b–f, the high-resolution XPS spectra of Ru, Ni, Mo, and O elements are provided. The high-resolution Ni 2p spectrum can be deconvoluted into two group peaks. The peaks at around 856.20 eV and 874.33 eV were the characteristic peaks of Ni^{2+}.[35] And, the peaks at 862.14 eV and 880.85 eV belonged to satellite peaks, which may derive from the surface oxidation of the catalyst.[36] The fitted curve of Mo 3d spectrum was deconvoluted into 232.16 eV and 235.28 eV, which corresponded to Mo^{6+}.[28,34,37] The binding energy of Ru $3p_{3/2}$ and $3p_{1/2}$ were located 463.39 eV and 485.62 eV.[14,23] Meanwhile, the high-resolution XPS spectra of Ru 3d and C 1s, the peaks with the energy of 284.75 eV and 281.18 eV could be assigned to Ru $3d_{3/2}$ and Ru $3d_{5/2}$,[35,38] indicating that Ru have been successfully incorporated into $NiMoO_4$–NF products. Besides, the binding energies of O 1s spectrum located at 532.47 eV and 530.68 eV, which were assigned to O–H of adsorbed water molecules and lattice oxygen.[28,39] By comparing the XPS of $Ru–NiMoO_4$–NF and $NiMoO_4$–NF (Fig. S5†), it is found that the binding energy of Ni, Mo, and O positively shift after the introduction of Ru. The results indicate that electrons are transferred from Ni, Mo, and O to Ru. Therefore, the interaction between Ru and substrate is the strong electron coupling effect.[40]

The HER electrocatalytic performances of $Ru–NiMoO_4$–NF, $NiMoO_4$–NF, and NF catalysts were evaluated in 1 M KOH solution under room temperature. As displayed in Fig. 5a, linear sweep voltammetric (LSV) curves of these three electrocatalysts indicated that the nickel foam was inert to HER. While $NiMoO_4$–NF performed poor HER activity. Remarkably, the $Ru–NiMoO_4$–NF catalyst exhibited enhanced remarkable HER activity in alkaline conditions after introducing Ru into $NiMoO_4$–NF. The overpotential of $Ru–NiMoO$–NF at 10 mA cm^{-2} is only 52 mV, which was considerably smaller than those of $NiMoO_4$–NF (249 mV), and NF (374 mV). Meanwhile, the electrocatalytic performance of Ru + $NiMoO_4$–NF was much worse than that of $Ru–NiMoO_4$–NF (Fig. S6†), indicating that forming heterojunctions can improve the catalytic activity, but

Fig. 4 XPS spectra of $Ru–NiMoO_4$–NF (a) full spectrum, (b) Ni 2p, (c) Mo 3d, (d) O 1s, (e) Ru 3d, and (f) Ru 3p.
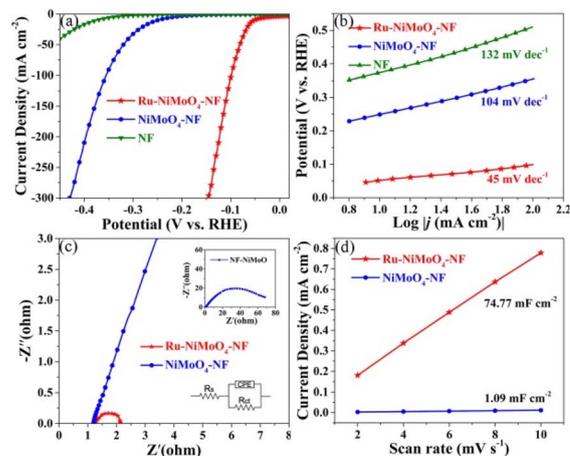

Fig. 5 (a) LSV curves, (b) Tafel slop curves, (c) EIS Nyquist plots, and (d) C_{dl} of different samples in 1 mol L^{-1} KOH.

not the simple drop coating on the surface. The HER kinetic behaviors and rate-determining step of the electrocatalysts were evaluated using Tafel plots.[4,14] The outstanding HER performance of Ru–NiMoO$_4$–NF was further confirmed by its much smaller Tafel slope (45 mV dec^{-1}) than those of NiMoO$_4$–NF (104 mV dec^{-1}), and NF (132 mV dec^{-1}) (Fig. 5b). This can be attributed to the favorable HER reaction kinetics on Ru–NiMoO–NF catalyst and Volmer–Heyrovsky mechanism. Meanwhile, the rate-determining step was the Heyrovsky step in the reaction process.

Furthermore, electrochemical impedance spectroscopy (EIS) was performed in order to better probe the charge transfer mechanism towards HER. The Nyquist plots were shown in Fig. 5c, the Ru–NiMoO$_4$–NF electrode presented a smaller semicircle and a lower charge transfer resistance (R_{ct}) value (0.42 Ω) than NiMoO$_4$–NF catalyst (37.78 Ω) in the low-frequency range, implying the faster of charge transfer and favorable reaction rate of HER.

The electrochemically active surface area (ECSA) was a good indicator to in-depth study the origin of the excellent activity, which was positively correlated with the electrochemical double-layer capacitance (C_{dl}). The C_{dl} value can be derived from the electrochemical cyclic voltammograms (CVs) measurement in the non-faradaic regions (Fig. S9†).[41,42] As displayed in Fig. 5d, Ru–NiMoO$_4$–NF had higher C_{dl} (74.77 mF cm^{-2}) than that of NiMoO$_4$–NF (1.09 mF cm^{-2}), implying Ru–NiMoO$_4$–NF had more active sites than NiMoO$_4$–NF. The mass activity of Ru–NiMoO$_4$–NF is 0.23 A mg$_{Ru}^{-1}$, which is larger than commercial Pt/C (0.18 A mg$_{pt}^{-1}$) at the overpotential of 70 mV.[4,22] In addition, long-time durability is a vital parameter for the catalyst in an electrochemical reaction.[28,43] Accordingly, the chronoamperometric measurement was carried out to further evaluate the electrocatalytic stability of Ru–NiMoO$_4$–NF and NiMoO$_4$–NF. As shown in Fig. 6a, the current density of Ru–NiMoO$_4$–NF was no apparent degradation even after 20 hours test. Simultaneously, the polarization curve did not show significant degradation after 3000 cyclic voltammetry cycles test (Fig. 6b). Furthermore, the morphology of Ru–NiMoO$_4$–NF after the stability test were well maintained (Fig. S11†). Meanwhile, the high resolution XPS of Ni, Mo, O, and Ru indicates no obvious change after HER tests (Fig. S12†). All these results demonstrate the excellent electrocatalytic stability of Ru–NiMoO$_4$–NF in alkaline.
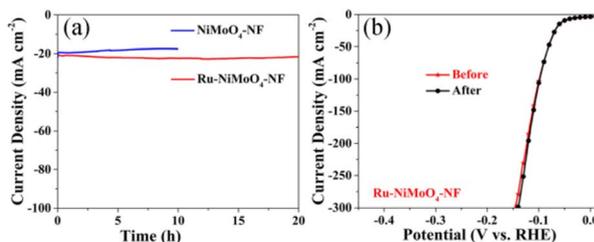

Fig. 6 Stability tests of Ru–NiMoO$_4$–NF and NiMoO$_4$–NF. (a) Chronoamperometry curves and (b) polarization curves.

Conclusions

In summary, ultralow Ru nanoparticles dispersed on α-NiMoO$_4$–NF nanorods electrocatalysts were successfully fabricated and exhibited highly efficient HER performance in alkaline media. The obtained Ru–NiMoO$_4$–NF showed an overpotential of 52 mV at the current density of 10 mA cm^{-2} and maintained stability over 20 h. The mass activity of Ru–NiMoO$_4$–NF is 0.23 A mg$_{Ru}^{-1}$, which is larger than commercial Pt/C (0.18 A mg$_{pt}^{-1}$). The unique heterostructures combined with Ru and α-NiMoO$_4$ boost the water dissociation kinetics and hydrogen evolution. This work provides an innovative way to construct transition metal oxide catalysts with trace noble metal content for HER.

Conflicts of interest

The authors declare no competing financial interest.

Acknowledgements

Notes and references

1 M. A. Ahsan, T. He, K. Eid, A. M. Abdullah, M. L. Curry, A. Du, A. R. Puente Santiago, L. Echegoyen and J. C. Noveron, Tuning the intermolecular electron transfer of low-dimensional and metal-free BCN/C$_{60}$ electrocatalysts via interfacial defects for efficient hydrogen and oxygen electrochemistry, *J. Am. Chem. Soc.*, 2021, **143**, 1203–1215.

2 Y. Xia, C. T. Campbell, B. Roldan Cuenya and M. Mavrikakis, Introduction: Advanced materials and methods for catalysis and electrocatalysis by transition metals, *Chem. Rev.*, 2021, **121**, 563–566.

3 S. Chu and A. Majumdar, Opportunities and challenges for a sustainable energy future, *Nature*, 2012, **488**, 294–303.

4 J. Wu, J. Fan, X. Zhao, Y. Wang, D. Wang, H. Liu, L. Gu, Q. Zhang, L. Zheng and D. J. Singh, Atomically dispersed MoOx on rhodium metallene boosts electrocatalyzed alkaline hydrogen evolution, *Angew. Chem., Int. Ed.*, 2022, **61**, e202207512.

5 L. Li, P. Wang, Q. Shao and X. Huang, Metallic nanostructures with low dimensionality for electrochemical water splitting, *Chem. Soc. Rev.*, 2020, **49**, 3072–3106.

6 X. Zhang, T. Liu, T. Guo, Z. Mu, X. Hu, K. He, X. Chen, V. P. Dravid, Z. Wu and D. Wang, High-performance MoC electrocatalyst for hydrogen evolution reaction enabled by surface sulfur substitution, *ACS Appl. Mater. Interfaces*, 2021, **13**, 40705–40712.

7 K. Liang, S. Pakhira, Z. Yang, A. Nijamudheen, L. Ju, M. Wang, C. I. Aguirre-Velez, G. E. Sterbinsky, Y. Du and Z. Feng, S-doped MoP nanoporous layer toward high-efficiency hydrogen evolution in pH-universal electrolyte, *ACS Catal.*, 2018, **9**, 651–659.

8 L. Wang, X. Duan, X. Liu, J. Gu, R. Si, Y. Qiu, Y. Qiu, D. Shi, F. Chen and X. Sun, Atomically dispersed Mo supported on metallic Co_9S_8 nanoflakes as an advanced noble-metal-free bifunctional water splitting catalyst working in universal pH conditions, *Adv. Energy Mater.*, 2020, **10**, 1903137.

9 G. Liu, F. Hou, S. Peng, X. Wang and B. Fang, Synthesis, physical properties and electrocatalytic performance of nickel phosphides for hydrogen evolution reaction of water electrolysis, *Nanomaterials*, 2022, **12**, 2935.

10 T. Terlouw, C. Bauer, R. McKenna and M. Mazzotti, Large-scale hydrogen production via water electrolysis: a techno-economic and environmental assessment, *Energy Environ. Sci.*, 2022, **15**, 3583–3602.

11 X. Lv, S. Wan, T. Mou, X. Han, Y. Zhang, Z. Wang and X. Tao, Atomic-level surface engineering of nickel phosphide nanoarrays for efficient electrocatalytic water splitting at large current density, *Adv. Funct. Mater.*, 2023, **33**, 2205161.

12 L. Yu, I. K. Mishra, Y. Xie, H. Zhou, J. Sun, J. Zhou, Y. Ni, D. Luo, F. Yu and Y. Yu, Ternary $Ni_{2(1-x)}Mo_{2x}P$ nanowire arrays toward efficient and stable hydrogen evolution electrocatalysis under large-current-density, *Nano Energy*, 2018, **53**, 492–500.

13 T. Wu, E. Song, S. Zhang, M. Luo, C. Zhao, W. Zhao, J. Liu and F. Huang, Engineering metallic heterostructure based on Ni_3N and 2M-MoS_2 for alkaline water electrolysis with industry-compatible current density and stability, *Adv. Mater.*, 2022, **34**, 2108505.

14 Q. Hu, K. Gao, X. Wang, H. Zheng, J. Cao, L. Mi, Q. Huo, H. Yang, J. Liu and C. He, Subnanometric Ru clusters with upshifted D band center improve performance for alkaline hydrogen evolution reaction, *Nat. Commun.*, 2022, **13**, 1–10.

15 Y. Zheng, Y. Jiao, A. Vasileff and S. Z. Qiao, The hydrogen evolution reaction in alkaline solution: from theory, single crystal models, to practical electrocatalysts, *Angew. Chem., Int. Ed.*, 2018, **57**, 7568–7579.

16 N. Mahmood, Y. Yao, J.-W. Zhang, L. Pan, X. Zhang and J.-J. Zou, Electrocatalysts for hydrogen evolution in alkaline electrolytes: mechanisms, challenges, and prospective solutions, *Adv. Sci.*, 2018, **5**, 1700464.

17 X. Wang, Y. Zheng, W. Sheng, Z. J. Xu, M. Jaroniec and S.-Z. Qiao, Strategies for design of electrocatalysts for hydrogen evolution under alkaline conditions, *Mater. Today*, 2020, **36**, 125–138.

18 D. Wang, T. Liu, J. Wang and Z. Wu, N, P (S) Co-doped Mo_2C/C hybrid electrocatalysts for improved hydrogen generation, *Carbon*, 2018, **139**, 845–852.

19 T. Liu, X. Zhang, T. Guo, Z. Wu and D. Wang, Boosted hydrogen evolution from α-MoC_{1-x}-MoP/C heterostructures, *Electrochim. Acta*, 2020, **334**, 135624.

20 J. K. Nørskov, T. Bligaard, A. Logadottir, J. Kitchin, J. G. Chen, S. Pandelov and U. Stimming, Trends in the exchange current for hydrogen evolution, *J. Electrochem. Soc.*, 2005, **152**, J23–J26.

21 Z. Wang, B. Xiao, Z. Lin, Y. Xu, Y. Lin, F. Meng, Q. Zhang, L. Gu, B. Fang and S. Guo, $PtSe_2$/Pt heterointerface with reduced coordination for boosted hydrogen evolution reaction, *Angew. Chem., Int. Ed.*, 2021, **60**, 23388–23393.

22 Y. Tan, J. Feng, H. Dong, L. Liu, S. Zhao, F. Lai, T. Liu, Y. Bai, I. P. Parkin and G. He, The edge effects boosting hydrogen evolution performance of platinum/transition bimetallic phosphide hybrid electrocatalysts, *Adv. Funct. Mater.*, 2022, **33**, 2209967.

23 Y. Sun, Z. Xue, Q. Liu, Y. Jia, Y. Li, K. Liu, Y. Lin, M. Liu, G. Li and C.-Y. Su, Modulating electronic structure of metal-organic frameworks by introducing atomically dispersed Ru for efficient hydrogen evolution, *Nat. Commun.*, 2021, **12**, 1–8.

24 Y. L. Wu, X. Li, Y. S. Wei, Z. Fu, W. Wei, X. T. Wu, Q. L. Zhu and Q. Xu, Ordered macroporous superstructure of nitrogen-doped nanoporous carbon implanted with ultrafine Ru nanoclusters for efficient pH-universal hydrogen evolution reaction, *Adv. Mater.*, 2021, **33**, 2006965.

25 Y. L. Wu, X. Li, Y. S. Wei, Z. Fu, W. Wei, X. T. Wu, Q. L. Zhu and Q. Xu, Ordered macroporous superstructure of nitrogen-doped nanoporous carbon implanted with ultrafine Ru nanoclusters for efficient pH-universal hydrogen evolution reaction, *Adv. Mater.*, 2021, **33**, 2006965.

26 B. You, Y. Zhang, Y. Jiao, K. Davey and S. Z. Qiao, Negative charging of transition-metal phosphides via strong electronic coupling for destabilization of alkaline water, *Angew. Chem., Int. Ed.*, 2019, **131**, 11922–11926.

27 S. Niu, W.-J. Jiang, Z. Wei, T. Tang, J. Ma, J.-S. Hu and L.-J. Wan, Se-doping activates FeOOH for cost-effective and efficient electrochemical water oxidation, *J. Am. Chem. Soc.*, 2019, **141**, 7005–7013.

28 Z. Wang, J. Chen, E. Song, N. Wang, J. Dong, X. Zhang, P. M. Ajayan, W. Yao, C. Wang and J. Liu, Manipulation on active electronic states of metastable phase β-$NiMoO_4$ for large current density hydrogen evolution, *Nat. Commun.*, 2021, **12**, 1–10.

29 Y. Zhu, Q. Lin, Y. Zhong, H. A. Tahini, Z. Shao and H. Wang, Metal oxide-based materials as an emerging family of hydrogen evolution electrocatalysts, *Energy Environ. Sci.*, 2020, **13**, 3361–3392.

30 L. An, J. Feng, Y. Zhang, R. Wang, H. Liu, G.-C. Wang, F. Cheng and P. Xi, Epitaxial heterogeneous interfaces on N-$NiMoO_4$/NiS_2 nanowires/nanosheets to boost hydrogen and oxygen production for overall water splitting, *Adv. Funct. Mater.*, 2019, **29**, 1805298.

31 P. Jiang, Y. Yang, R. Shi, G. Xia, J. Chen, J. Su and Q. Chen, Pt-like electrocatalytic behavior of Ru–MoO_2 nanocomposites for the hydrogen evolution reaction, *J. Mater. Chem. A*, 2017, **5**, 5475–5485.

32 L. Zhang, Z. Hu, H. Li, Q. Ren, Y. Qiu, J. Qu and S. Hu, Nickel foam supported NiO@Ru heterostructure towards high-efficiency overall water splitting, *ChemPhysChem*, 2021, **22**, 1785–1791.

33 Y. Wang, P. Zheng, M. Li, Y. Li, X. Zhang, J. Chen, X. Fang, Y. Liu, X. Yuan, X. Dai and H. Wang, Interfacial synergy between dispersed Ru sub-nanoclusters and porous NiFe layered double hydroxide on accelerated overall water splitting by intermediate modulation, *Nanoscale*, 2020, **12**, 9669–9679.

34 Y. Y. Chen, Y. Zhang, X. Zhang, T. Tang, H. Luo, S. Niu, Z. H. Dai, L. J. Wan and J. S. Hu, Self-templated fabrication of $MoNi_4/MoO_{3-x}$ nanorod arrays with dual active components for highly efficient hydrogen evolution, *Adv. Mater.*, 2017, **29**, 1703311.

35 G. Chen, T. Wang, J. Zhang, P. Liu, H. Sun, X. Zhuang, M. Chen and X. Feng, Accelerated hydrogen evolution kinetics on NiFe-layered double hydroxide electrocatalysts by tailoring water dissociation active sites, *Adv. Mater.*, 2018, **30**, 1706279.

36 L. Zhang, H. Wei, H. Jiu, C. Wang, Y. Qin, S. Che, Z. Guo and Y. Han, Ni_3N/Co_4N nanosheet heterojunction electrocatalyst for hydrogen evolution reaction in alkaline fresh water/simulated seawater, *Dalton Trans.*, 2022, **51**, 16733–16739.

37 L. Guo, J. Chi, J. Zhu, T. Cui, J. Lai and L. Wang, Dual-doping $NiMoO_4$ with multi-channel structure enable urea-assisted energy-saving H_2 production at large current density in alkaline seawater, *Appl. Catal., B*, 2023, **320**, 121977.

38 L.-N. Zhang, Z.-L. Lang, Y.-H. Wang, H.-Q. Tan, H.-Y. Zang, Z.-H. Kang and Y.-G. Li, Cable-like Ru/WNO@C nanowires for simultaneous high-efficiency hydrogen evolution and low-energy consumption chlor-alkali electrolysis, *Energy Environ. Sci.*, 2019, **12**, 2569–2580.

39 C. Chen, S. He, K. Dastafkan, Z. Zou, Q. Wang and C. Zhao, Sea urchin-like $NiMoO_4$ nanorod arrays as highly efficient bifunctional catalysts for electrocatalytic/photovoltage-driven urea electrolysis, *Chin. J. Catal.*, 2022, **43**, 1267–1276.

40 M. Yang, Y. Jiang, M. Qu, Y. Qin, Y. Wang, W. Shen, R. He, W. Su and M. Li, Strong electronic couple engineering of transition metal phosphides-oxides heterostructures as multifunctional electrocatalyst for hydrogen production, *Appl. Catal., B*, 2020, **269**, 118803.

41 Y. Wu, X. Liu, D. Han, X. Song, L. Shi, Y. Song, S. Niu, Y. Xie, J. Cai and S. Wu, Electron density modulation of $NiCo_2S_4$ nanowires by nitrogen incorporation for highly efficient hydrogen evolution catalysis, *Nat. Commun.*, 2018, **9**, 1–9.

42 M. Yang, Y. Jiang, S. Liu, M. Zhang, Q. Guo, W. Shen, R. He, W. Su and M. Li, Regulating the electron density of dual transition metal sulfide heterostructures for highly efficient hydrogen evolution in alkaline electrolytes, *Nanoscale*, 2019, **11**, 14016–14023.

43 J. Zhang, Y. Zhao, X. Guo, C. Chen, C.-L. Dong, R.-S. Liu, C.-P. Han, Y. Li, Y. Gogotsi and G. Wang, Single platinum atoms immobilized on an MXene as an efficient catalyst for the hydrogen evolution reaction, *Nat. Catal.*, 2018, **1**, 985–992.